RESEARCH PAPER

Evaluation of chemo-photodynamic therapy of multi-drug (metformin-methylene blue) conjugated to ferrofluidic nanocarrier on triple-negative breast cancer cells in hyperglycemic conditions

Samaneh B. Chalaki[1], Mostafa Gholizadeh[*1], Batool Akhlaghinia[1], Armin Imanparast[2,3], Ameneh Sazgarnia[2,3]

[1] Department of Chemistry, Faculty of Science, Ferdowsi University of Mashhad, Mashhad, Iran
[2] Medical Physics Research Center, Basic Sciences Research Institute, Mashhad University of Medical Sciences, Mashhad, Iran
3 Department of Medical Physics, Faculty of Medicine, Mashhad University of Medical Sciences, Mashhad, Iran

ABSTRACT

Objective(s): Previous studies have established a link between hyperglycemia (high blood sugar) and hyperinsulinemia (elevated insulin levels) in diabetes, and the subsequent promotion of cancer cell growth. Among various cancers, triple-negative breast cancer (TNBC) is one of the most aggressive types, which can exhibit heightened malignancy in the presence of diabetes. The objective of this study is to introduce a novel approach to combined chemo-photodynamic therapy (Ch-PDT) for TNBC, utilizing metformin (MET) and methylene blue (MB) conjugated to a ferrofluidic nanocarrier, targeting MDA-MB-231 breast cancer cells under conditions that simulate high blood sugar.

Material and methods: To this end, Fe_3O_4f nanoparticles were synthesized via the hydrothermal method and subsequently modified with polyethylene glycol and 3-aminopropyltriethoxysilane (APTES) to enhance drug loading efficiency. The physicochemical properties of the nanoparticles were characterized using FT-IR, XRD, FE-SEM, TEM, EDX, ^{1}H-NMR, VSM, and UV-VIS spectroscopy. For the Ch-PDT application, the cells were incubated with the different formulations and subjected to various irradiation conditions. Cell viability was then assessed for all treatment groups using the MTT assay.

Results: Increased exposure in the MB-containing group resulted in reduced cell survival, likely due to the photosensitizing properties of methylene blue. However, in the Fe_3O_4f-PEG-MET-MB group, cell death increased significantly as the irradiation time was extended. This synergistic effect is attributed to the enhanced efficacy of combined chemo-photodynamic therapy (Ch-PDT), which optimizes the therapeutic potential of metformin ($P < 0.01$).

Conclusion: Based on the results, Ch-PDT can be an effective method in increasing the efficiency of metformin in inhibiting metastatic breast cancer tumor cells in hyperglycemic conditions.

Keywords: *Hyperglycemia, Metformin, Methylene blue, Photodynamic therapy, Breast cancer*

How to cite this article
Chalaki SB, Gholizadeh M, Akhlaghinia B, Imanparast A, Sazgarnia A. Evaluation of chemo-photodynamic therapy of multi-drug (metformin-methylene blue) conjugated to ferrofluidic nanocarrier on triple-negative breast cancer cells in hyperglycemic conditions. Nanomed J. 2025; 12: 1-. DOI: 10.22038/NMJ.2025.82375.2055

INTRODUCTION

More than three-quarters of global mortality is attributed to non-communicable diseases (NCDs), including cardiovascular diseases (such as stroke and myocardial infarction), chronic respiratory diseases, cancers, and diabetes [1]. In the United States, over 200,000 new cases of breast cancer are diagnosed annually, with approximately 40,000 resulting in death from the disease [2].

Numerous epidemiological studies have established a connection between diabetes and an increased risk of breast cancer. These studies have demonstrated that breast cancer patients with diabetes face a 50% higher risk of mortality compared to those without diabetes [3]. Hyperglycemia and hyperinsulinemia in diabetic patients have been linked to cancer cell growth through various mechanisms. Elevated insulin levels directly promote cancer cell growth by binding to insulin receptors, particularly in cancers that express high levels of these receptors [4, 5]. In addition, hyperinsulinemia can increase levels of insulin-like growth factors (IGF), further stimulating cancer cell growth and survival through IGF receptors [5, 6]. High blood sugar also triggers chronic inflammation, creating a cancer-friendly environment by promoting cell proliferation and angiogenesis [7-9]. Moreover, the production of reactive oxygen species (ROS) induced by hyperglycemia can lead to DNA damage and genetic mutations, contributing to cancer development [10]. Prolonged hyperglycemia and hyperinsulinemia further impair the immune

*Corresponding author(s) Email: m_gholizadeh@um.ac.ir
Note. This manuscript was submitted on September 07, 2024; approved on January 22, 2025.

response to cancer cells, facilitating their evasion and proliferation. Additionally, disruptions in hormone balance, including sex hormones such as estrogen and testosterone, may influence cancer cell growth, particularly in hormone-sensitive cancers [11-13].

Breast cancer patients may develop hyperglycemia (high blood sugar) as a result of cancer treatments, including chemotherapy and hormonal therapy. Certain chemotherapy drugs, such as steroids, taxanes, platinum compounds, and 5-fluorouracil (5FU), can elevate blood sugar levels [14-16]. dditionally, hormonal therapies like tamoxifen and aromatase inhibitors are also associated with an increased risk of hyperglycemia. This condition is concerning for breast cancer patients as it can lead to complications, including poor wound healing, infections, and cardiovascular disease. Furthermore, patients with pre-existing diabetes may experience worsened glycemic control during cancer treatment [17, 18]. Therefore, breast cancer patients need to be closely monitored for hyperglycemia, and appropriate lifestyle interventions, such as diet and exercise, should be implemented to manage blood sugar levels during treatment.

Metformin is a multifunctional oral medication primarily used to treat type 2 diabetes [19] and has demonstrated significant potential in the prevention and treatment of breast cancer [20, 21]. In type 2 diabetes, metformin improves glucose homeostasis and reduces hyperinsulinemia, mechanisms that help mitigate the risk factors associated with the development of insulin-sensitive cancers [22]. In addition, metformin directly targets cancer cells by inhibiting respiratory chain complex I, thereby reducing oxidative respiration and disrupting the ATP/AMP ratio. This imbalance is beneficial for enhancing chemodynamic therapy [23, 24].

Chemo-photodynamic therapy (Ch-PDT) is an emerging cancer treatment that combines a photosensitizer drug with a complementary agent to increase reactive oxygen species (ROS) production. Metformin, a medication commonly used to treat type 2 diabetes, has been shown to enhance oxygen availability in cells and tissues, thereby sensitizing cancer cells to ROS during Ch-PDT. Metformin inhibits the mitochondrial respiratory chain, leading to increased adenosine monophosphate (AMP) levels and activation of AMP-activated protein kinase (AMPK). This activation promotes glucose uptake and fatty acid oxidation. Additionally, AMPK activation has been shown to improve oxygen delivery to cells, further enhancing the effectiveness of Ch-PDT. Metformin also reduces antioxidant levels in cancer cells, making them more vulnerable to ROS-induced cell death, thereby potentially improving the efficacy of this therapy in cancer treatment [25, 26]. Several studies have demonstrated that metformin inhibits the proliferation of BT474, BT20, MDA-MB-453, T47D, and MCF7 breast cancer cells through a pathway independent of estrogen receptor (ER) or human epidermal growth factor receptor-2 (HER2) signaling, inducing caspase-dependent cell death (4). However, some researchers have reported that metformin does not affect the anti-proliferative activity or apoptosis induction in MDA-MB-231 triple-negative invasive breast cancer cells [27-29]. The underlying explanation for this phenomenon is that MDA-MB-231 cells lack the LKB1 factor, which is essential for activating AMPK. Consequently, these cells are resistant to the anticancer effects of metformin [29].

Despite the relatively large surface area of magnetic nanostructures, which makes them suitable for surface modification of multidrug nanocarriers, their development has been challenging due to issues with colloidal stability and the tendency to aggregate in the bloodstream, owing to their instability [30, 31]. These challenges have restricted their use primarily to pre-clinical research.

In addition to the chemotherapy drug metformin, the photosensitizer methylene blue was also utilized in photodynamic therapy (PDT). Methylene blue is of significant interest as a photosensitizer in the PDT of breast cancer due to its ability to absorb light at higher wavelengths (which allows for better penetration depth), its efficient ROS production, biocompatibility, low cost, and high availability for both laboratory and clinical applications.

In this study, Fe_3O_4 ferrofluid was used for the first time as a magnetic core in drug delivery. Fe_3O_4 ferrofluid is a stable suspension of magnetic particles, ranging from nanometers to micrometers, suspended in a carrier liquid, which can be either oil- or water-based [32, 33]. Metformin and methylene blue (MB) were immobilized on the surface of the Fe_3O_4f core through a polyethylene glycol 2000 (PEG-2000) linker. The combined chemo-photodynamic therapy (Ch-PDT) was then evaluated in the aggressive MDA-MB-231 cancer cell line under hyperglycemic conditions. The primary aim of this project was to investigate the chemo-

photodynamic characteristics of the engineered nanostructure, with minimal emphasis on its magnetic properties. However, future studies will focus on exploiting the magnetic properties of this nanostructure for combined therapeutic interventions, due to its promising potential demonstrated in this investigation. By integrating magnetic hyperthermia with ionizing and non-ionizing radiation methods, the goal is to create novel treatment strategies that offer precise, synergistic therapeutic effects, thus advancing the field of nanomedicine and improving treatment efficacy for pathological conditions.

MATERIALS AND METHODS

Chemical reagents

Polyethylene glycol (PEG, Mw = 2000 g/mol), Dulbecco's modified Eagle's medium (DMEM) base, methylene blue (MB, Mw = 319.85 g/mol), MTT (3-(4,5-dimethylthiazol-2-yl)-2,5-diphenyltetrazolium bromide), 1,3-diphenylisobenzofuran (DPBF), metformin (MET) (Alborz-Bulk Pharmaceutical Company, Tehran, Iran), penicillin, trypsin–EDTA, fetal bovine serum (FBS), trypan blue, and streptomycin were purchased from Sigma-Aldrich (St. Louis, MO, USA). Additionally, all chemical reagents and solvents used in this study were obtained from Merck Chemical Corporation and were used as received, without further purification.

Instruments

The FT-IR spectra were recorded using pressed KBr pellets with an AVATAR 370 FT-IR spectrometer (Thermo Nicolet, USA) at room temperature, covering a range from 4000 to 400 cm^{-1} with a resolution of 4 cm^{-1}. NMR spectra were obtained on Bruker Avance 300 and 400 MHz instruments in DMSO-d_6.

The crystalline structure of the catalyst was examined using X-ray diffraction (XRD) with a D8 ADVANCE-Bruker diffractometer, operated at 40 kV and 30 mA, utilizing Cu Kα radiation (λ = 0.154 nm).

Transmission electron microscopy (TEM) analysis was conducted with a Leo 912 AB microscope (Zeiss, Germany) at an accelerating voltage of 120 kV. Elemental compositions were determined using a Leo 1450 VP scanning electron microscope, equipped with an SC7620 energy dispersive spectrometer (SEM-EDS), which provides a resolution of 133 eV at 20 kV.

Dynamic light scattering (DLS) analysis was performed using a Zetasizer Nano ZS from Malvern Instruments to assess the particle size distribution in a colloidal suspension. Additionally, zeta potential (ζ) measurements were conducted with the same Zetasizer Nano ZS system (Malvern Instruments Ltd, Malvern, UK). These measurements are essential for determining the point of zero charge (pH$_x$), which is the pH at which the net surface charge of the particles becomes neutral. This information is crucial for understanding the stability and behavior of colloidal systems in various applications.

The magnetic properties of the catalyst were evaluated using a vibrating sample magnetometer (VSM) from Magnetic Danesh Pajoh Institute, allowing precise measurement of the material's magnetic behavior.

Additionally, inductively coupled plasma atomic emission spectroscopy (ICP-OES) was performed using a Varian VISTA-PRO instrument equipped with a charge-coupled device (CCD) from Australia. This technique is essential for determining the elemental composition of the catalyst by analyzing the emitted light from plasma-excited atoms. Furthermore, product yields were reported after isolating the products, which were purified via recrystallization. This step is critical for ensuring the purity and quality of the final products obtained from the synthesis.

Synthesis of Fe3O4 f-PEG-MET@MB

Preparation of Fe_3O_4 fluidic (Fe_3O_4 f)

Magnetite nanoparticles were synthesized in a two-necked flask equipped with an argon gas inlet tube, following a method reported previously with minor modifications. In this process, 1 mmol of $C_6H_5Na_3O_7 \cdot 2H_2O$, 2 mmol of $NaNO_3$, and 4 mmol of NaOH were dissolved in 19 mL of deionized water and distilled water, and the solution was heated on a stove at 100°C. Subsequently, 1 mL of 2 M $FeSO_4 \cdot 7H_2O$ was added rapidly. The resulting suspension was stirred for 1 hour to allow the chemical reaction to proceed. The black precipitate formed was separated using an external magnet and washed several times with water [32].

Synthesis of HOOC-PEG-triethoxysilane (HOOC-PEG silane)

Five mmol of PEG 2000, 10 mmol of succinic anhydride, and 0.12 g of 4-dimethylaminopyridine were dissolved in 30 mL of dichloromethane and heated under reflux conditions for 3 hours. Then, 5 mmol of thionyl chloride was added to the PEG-carboxylate solution at 30°C. The pH of the solution was subsequently adjusted to 5 using triethylamine. Next, 5 mmol of 3-aminopropyltriethoxysilane was added to the mixture at ambient temperature, and the mixture was stirred for 10 hours. The HOOC-PEG-triethoxysilane was then crystallized using isopropyl ether and dried under vacuum. The

synthesis of HOOC-PEG-triethoxysilane is depicted in Scheme 1 [34].

The dried material was dissolved in deionized water and dialyzed against deionized water for 2 days to remove unreacted materials. The solution was then lyophilized for 3 days. The structure of HOOC-PEG-silane was confirmed using ^{1}H NMR spectroscopy [35, 36].

Preparation of Fe_3O_4f-PEG

Subsequently, the synthesized Fe_3O_4f was dispersed in deionized water, and activated polyethylene glycol was added to the solution. The mixture was then placed on a shaker for 24 hours. Afterward, the upper solution was separated by centrifugation and prepared for the next phase, which involved drying using a freeze dryer.

Preparation of Fe_3O_4f-PEG-MET

Metformin was added to a dimethyl sulfoxide (DMSO) solution containing a 1.2 molar equivalent of N,N′-Dicyclohexylcarbodiimide (DCC) and N-hydroxysuccinimide (NHS). The mixture was stirred for 24 hours at 25°C, after which the solution was centrifuged at 4000 × g for 5 minutes to precipitate the Fe_3O_4f-PEG-MET complex [37-39] (Scheme 2).

Preparation of Fe3O4f-PEG-MET@MB

Blending methylene blue (MB) with Fe_3O_4f-PEG-MET facilitates hydrogen bonding between MB and PEG-MET. Based on this interaction, the photosensitive MB compound is added to the solution before administering the treatment. This combination has been utilized to employ Fe_3O_4f in chemo-photodynamic therapy (Ch-PDT) [40, 41].

Reactive oxygen species (ROS) dosimetry

Studies have shown that 1,3-diphenylisobenzofuran (DPBF), a well-known ROS dosimeter in photodynamic therapy, primarily reacts with singlet oxygen. The presence of singlet oxygen ($^1O_2$) is detected through the bleaching of DPBF [42, 43].

For the evaluation of $^1O_2$ dosimetry, a stock solution of DPBF (concentration 0.115 mM) was prepared in ethanol. All therapeutic groups were also prepared in water (Analyte in water/DPBF ratio = 2:1) and analyzed using spectrophotometry after irradiation.

Cell culture

MDA-MB-231 cells were cultured in DMEM with a high glucose formulation (25 mM) to simulate diabetic-like conditions, supplemented with 10% fetal bovine serum (FBS). The cultures were maintained at 37°C in a 5% CO_2 atmosphere. The culture medium was supplemented with penicillin (100 units/mL) and streptomycin (100 µg/mL) to maintain sterility. After 72 hours of growth, the cells were detached from the flask using trypsinization to achieve the desired cell count. Cell viability and counting were assessed using the Trypan Blue exclusion method. Subsequently, the MDA-MB-231 cells were plated into 24-well plates at a density of 7×10^4 cells per well and incubated in the CO_2 incubator for 24 hours.

In-vitro Chemo-photodynamic therapy

To determine the maximum non-toxic concentration of the compounds used in the biological environment, cells were counted and seeded into 24-well plates. After 24 hours, the cells were incubated with different concentrations of MET, MB, Fe_3O_4f-PEG, Fe_3O_4f-PEG-MET, and Fe_3O_4f-PEG-MET@MB for 180 minutes. Following incubation, the cells were washed with PBS, and 48 hours after the removal of the drugs and therapeutic compounds, the MTT assay was performed to assess cytotoxicity. This assay evaluates the activity of mitochondrial dehydrogenases to determine the viability of the cells after treatment.

Cell counts were performed after a 24-hour incubation, followed by seeding the cells into a 24-well plate to determine the highest non-toxic concentration of the compounds used in the biological setting. The cells were then exposed to varying concentrations of MET, MB, Fe_3O_4f-PEG, Fe_3O_4f-PEG-MET, and Fe_3O_4f-PEG-MET@MB for 180 minutes. After incubation, the cells were rinsed with phosphate-buffered saline (PBS). Forty-eight hours after removing the drugs and therapeutic agents, an MTT assay was conducted to assess cytotoxicity. This assay evaluates the activity of mitochondrial dehydrogenases, providing insight into the viability and metabolic activity of the cells after exposure to the agents over the 48 hours.

Twenty-four hours after cell seeding, the culture medium was replaced with fresh medium containing varying concentrations of drug agents (MET, MB, Fe_3O_4f-PEG, Fe_3O_4f-PEG-MET, and Fe_3O_4f-PEG-MET@MB) (MB concentration: 20 µM, metformin: 1 mM). After a 180-minute incubation, the plates were rinsed with phosphate-buffered saline (PBS) to remove any excess unabsorbed drugs. Fresh culture medium containing 3% fetal bovine serum (FBS) was added to each well. The cells were subsequently subjected to varying levels of radiant exposure: 2682 and 5364 mJ/cm², at a wavelength of 600 nm. Following irradiation, a new culture medium with 17% FBS was introduced to the wells, adjusting the average FBS concentration to 10% [(3% + 17%)/2]. The cells were incubated for an

additional 24 hours. Finally, an MTT assay was performed on all treatment groups 48 hours post-irradiation to evaluate cell viability and metabolic activity.

MTT assay

The MTT assay was performed on all treatment groups 48 hours after irradiating the cells. Before the assay, the cells were examined under a microscope to assess their morphology, confirming growth or death rates in both the control and treatment groups, and ensuring no microbial contamination. The culture medium was then carefully removed under a laminar flow hood. Next, 500 µl of FBS-free culture medium and 50 µl of MTT solution were added to each well in a dark environment. The plates were covered with aluminum foil to protect them from light and incubated for 4 hours. After incubation, the supernatant was discarded, and 1000 µl of dimethyl sulfoxide (DMSO) was added to dissolve the formazan crystals. To ensure homogeneity, each plate was placed on a shaker for 5 minutes. Finally, to measure cytotoxicity, the contents of each well in the 24-well plate were transferred equally to a 96-well plate, and the absorbance was measured using an ELISA reader at wavelengths of 570 nm and 630 nm.

Evaluation indices

Treatment Efficacy (TE)

The treatment efficacy index (TE) is defined to assess the effectiveness of photodynamic therapy (PDT) involving the Fe_3O_4f-PEG-MET@MB formulation. This index is calculated as the ratio of radiation-induced cell death (CD) in the presence of Fe_3O_4f-PEG-MET@MB to the radiation-induced cell death in the presence of MB alone [44].

$$TE\ (Fe_3O_4f\text{-}PEG\text{-}MET@MB) = \frac{CD_{Fe_3O_4\text{f-PEG-MET@MB}}}{CD_{\text{MB}}}$$

Synergism ratio (SYN)

The synergism ratio is a quantitative metric used to assess the combined effectiveness of a treatment formulation compared to its components [44]. Specifically, for the Fe_3O_4f-PEG-MET@MB formulation, the synergism ratio is calculated as the ratio of radiation-induced cell death in the presence of Fe_3O_4f-PEG-MET@MB to the total radiation-induced cell death observed when each component (Fe_3O_4f-PEG, MET, and MB) is administered separately. A synergism ratio (Syn) greater than 1 indicates that the combined treatment is more effective at inducing cell death than the sum of its components, suggesting a synergistic effect. In contrast, a ratio of 1 or less suggests that the combined treatment does not offer additional benefits beyond the individual components. This index is crucial for evaluating the potential advantages of combination therapies in enhancing therapeutic efficacy. For the Fe_3O_4f-PEG-MET@MB formulation, the synergism ratio can be defined mathematically as follows:

$$Syn\ (Fe_3O_4f\text{-}PEG\text{-}MET@MB) = \frac{CD_{Fe_3O_4\text{f-PEG-MET@MB}}}{CD_{\text{MB}} + CD_{\text{MET}} + CD_{Fe_3O_4f-PEG}}$$

Statistical analysis

In this study, data analysis was performed using SPSS version 22. To assess the normality of the data, the Kolmogorov-Smirnov test, a nonparametric goodness-of-fit test, was employed. Following this, one-way ANOVA was used to analyze statistical differences among all treatment groups. Tukey's multiple comparison tests were then conducted to identify specific group differences, with a significance level set at $P < 0.05$. This statistical approach allowed for a comprehensive evaluation of the treatment effects across the different groups in the study.

RESULTS

In the first section of this paper, the preparation of Fe_3O_4f-PEG-MET@MB was characterized using various analytical techniques, including XRD, VSM, FT-IR, TEM, FE-SEM-EDS, UV-Vis spectrophotometry, ^{1}H NMR spectroscopy, and ICP-OES.

UV-visible spectrophotometry

A UV spectrum scan was conducted to confirm and validate the interaction between MB, metformin, and the Fe_3O_4f-PEG-MET combination. Due to the hydrogen bonding between PEG-MET and MB, as depicted in Scheme 3, the λmax of their spectrum exhibited a red shift compared to metformin alone (Figure 1a). UV-Visible spectroscopy measurements revealed that the amount of metformin conjugated to Fe_3O_4f-PEG reached a saturation concentration of 21.4% metformin in Fe_3O_4f-PEG-MET (Figure 1b).

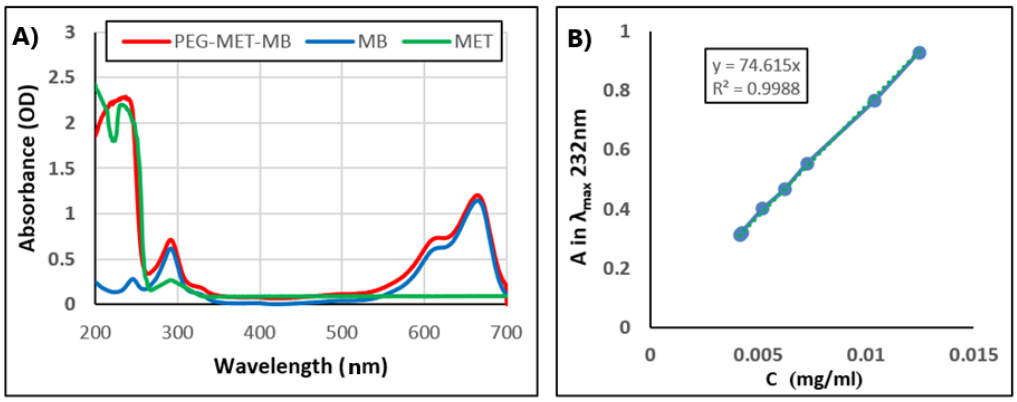

Fig. 1. A) UV Spectrum methylene Blue (Blue line), metformin (green line) and Fe_3O_4f-PEG-MET-MB (Red line). B) Metformin concentration standard curve. (**MB**: Methylene Blue, **PEG**: Polyethylene glycol, **MET**: Metformin).

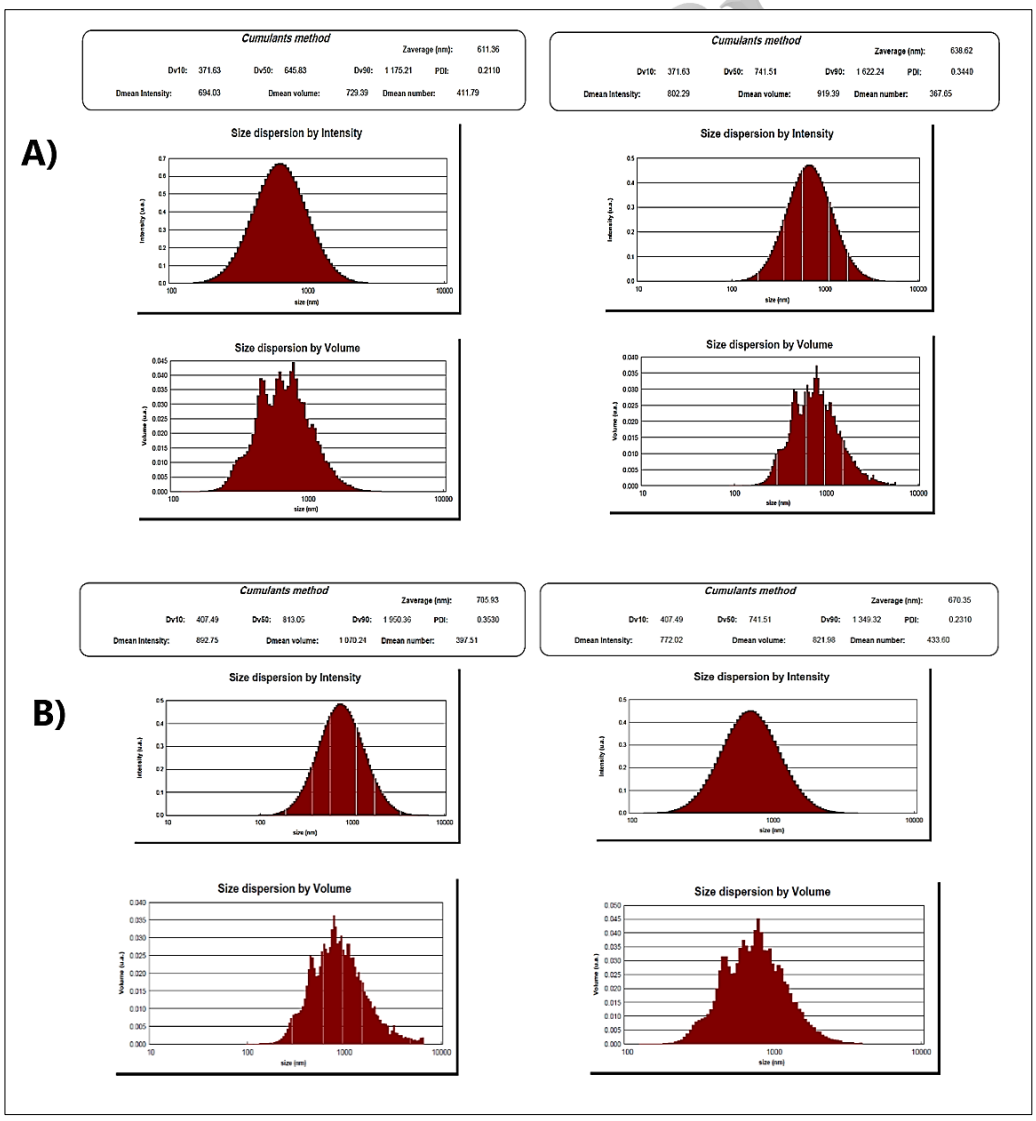

Fig. 2. Size of nanoparticles based on Dynamic Light Scattering (DLS) for **A) Fe_3O_4f-PEG**-MET and **B) Fe_3O_4f-PEG**-MET@MB. (**MB**: Methylene Blue, **PEG**: Polyethylene glycol, **MET**: Metformin)

Particle size/morphology/zeta potential analysis

To determine the hydrodynamic diameter distribution of the synthesized nanoparticles, dynamic light scattering (DLS) analysis was performed. The average sizes of Fe_3O_4f-PEG-MET and Fe_3O_4f-PEG-MET@MB nanoparticles were found to be 748 nm and 832 nm, respectively, with a polydispersity index (PDI) of 0.29. This low PDI value indicates a relatively uniform and stable nanoparticle dispersion in solution (Figure 2).

Furthermore, zeta potential measurements revealed a significant decrease in surface charge, from +10.58 mV to -28.35 mV for Fe_3O_4f-PEG-MET and Fe_3O_4f-PEG-MET@MB, respectively (Figure 3). This negative shift in zeta potential suggests successful surface modification with methylene blue, resulting in a negatively charged nanoparticle surface. A high absolute value of zeta potential typically indicates improved colloidal stability, reducing the likelihood of nanoparticle aggregation.

Furthermore, transmission electron microscopy (TEM) was employed to obtain direct information about the nanostructure and morphology of Fe_3O_4f and Fe_3O_4f-PEG-MET. Figures 4 and 5 show the TEM images and particle size distributions of the synthesized Fe_3O_4f. As shown in Figure 4b, core-shell nanoparticles were synthesized, and to further confirm the particle size, DLS analysis was performed. Additionally, the size distribution histogram of Fe_3O_4f indicated that the average diameter of the nanoparticles was 80–100 nm, which is consistent with the results obtained from XRD (Figure 5).

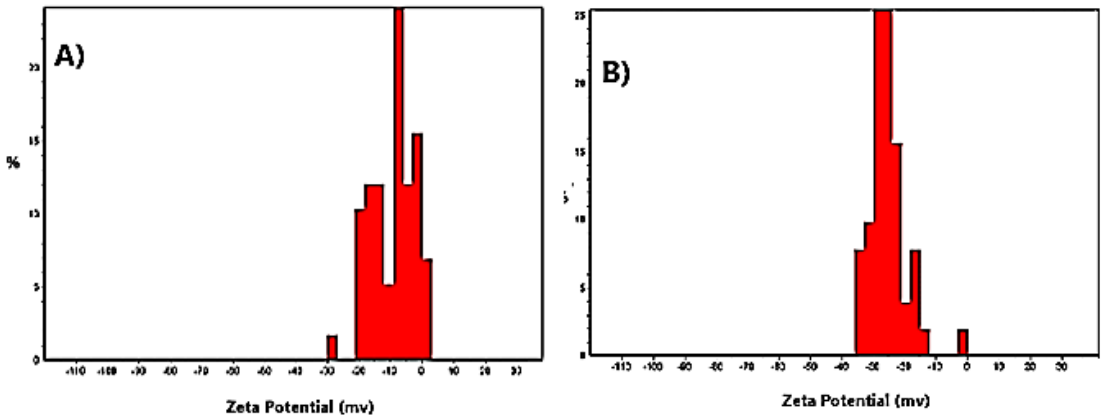

Fig. 3. Zeta potential of **A)** Fe_3O_4f-PEG-MET **B)** Fe_3O_4f-PEG-MET@MB. (**MB**: Methylene Blue, **PEG**: Polyethylene glycol, **MET**: Metformin)

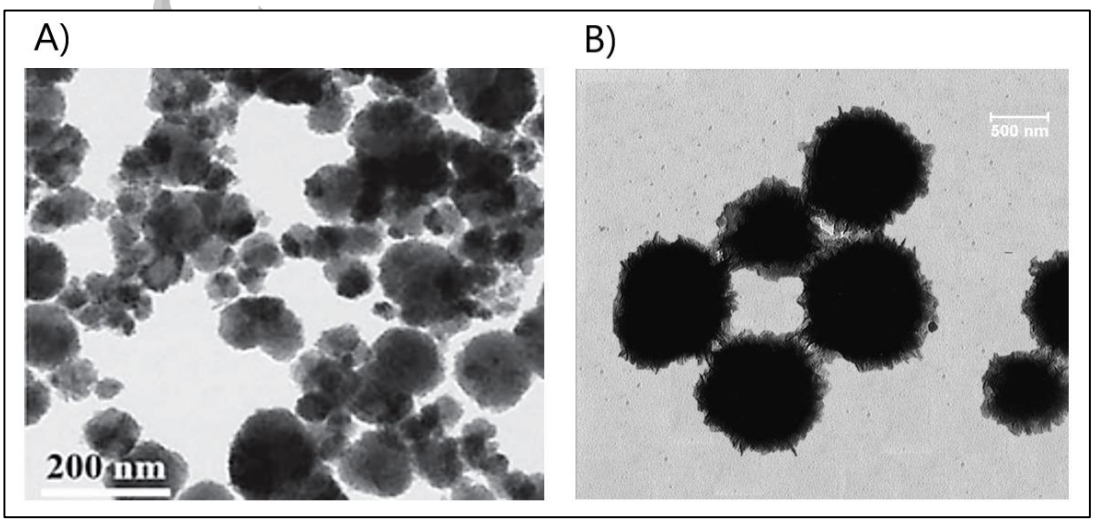

Fig. 4. TEM images of A) Fe_3O_4 and B) Fe_3O_4f-PEG-MET-MB (**MB**: Methylene Blue, **PEG**: Polyethylene glycol, **MET**: Metformin)

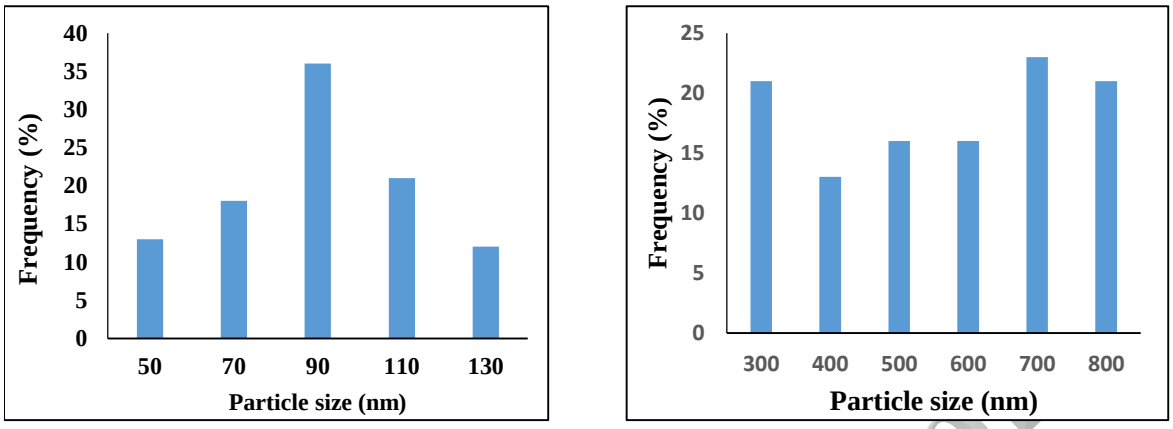

Fig. 5. Particle size distribution histogram of A) Fe_3O_4 fluidic B) Fe_3O_4f-PEG-MET

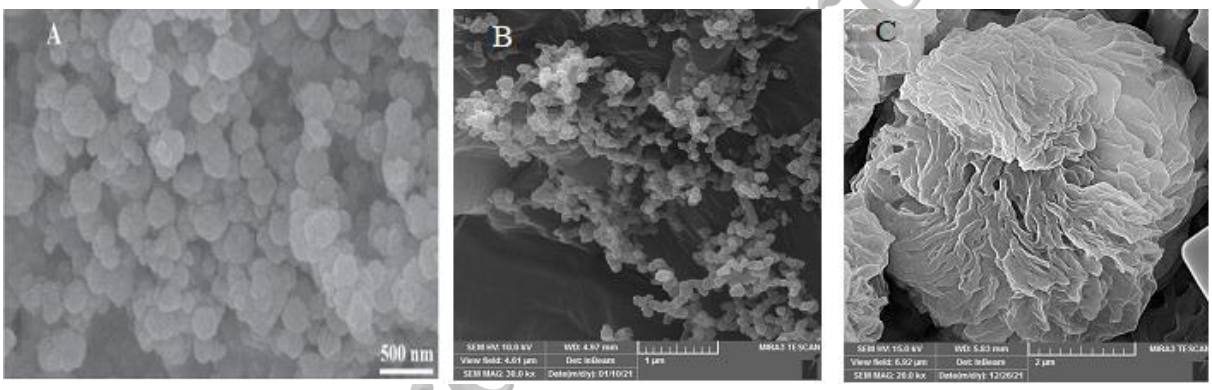

Fig. 6. FE SEM images of A) Fe_3O_4, B) HOOC-PEG-triethoxysilane, C) Fe_3O_4f-PEG-MET

The morphology of Fe_3O_4f NPs, HOOC-PEG-triethoxysilane, and Fe_3O_4f-PEG-MET was also examined using the FE-SEM technique. As shown in Figure 6a, the as-synthesized Fe_3O_4f NPs exhibited spherical and irregular morphologies with good dispersion. In Figure 6c, three-dimensional structures resembling tree-like formations are observed, with branches that can be extended by polymerizing the central molecule. The drug molecules are positioned on the surface or between the branches of these structures.

Discrepancies in particle size measurements obtained from DLS compared to TEM and SEM can be attributed to the inherent differences in their measurement techniques and environments. DLS, an intensity-based technique used in liquid suspensions, is more sensitive to larger particles and accounts for the solvated layer around the particle, which inflates the apparent size. In contrast, TEM and SEM directly image dry samples, providing a number-based measurement of the true particle size without the influence of the solvent layer or potential agglomeration effects. While DLS offers valuable insights into the hydrodynamic diameter, combining it with microscopy techniques is often employed for a more comprehensive understanding of particle size distribution and morphology.

Characterization of Fe_3O_4-PEG-ME@MB

HOOC-PEG-triethoxysilane (HOOC-PEG silane) was analyzed by ^{1}H NMR spectroscopy, and the results are shown in Figure 7. ^{1}H NMR ($CDCl_3$, 300 MHz) δ in ppm: 3.6 (triplet of triplets, CH_2), 0.9 (triplet, CH_3), 7.6–7.7 (1H, triplet, NH), 13–15 (singlet, OH).

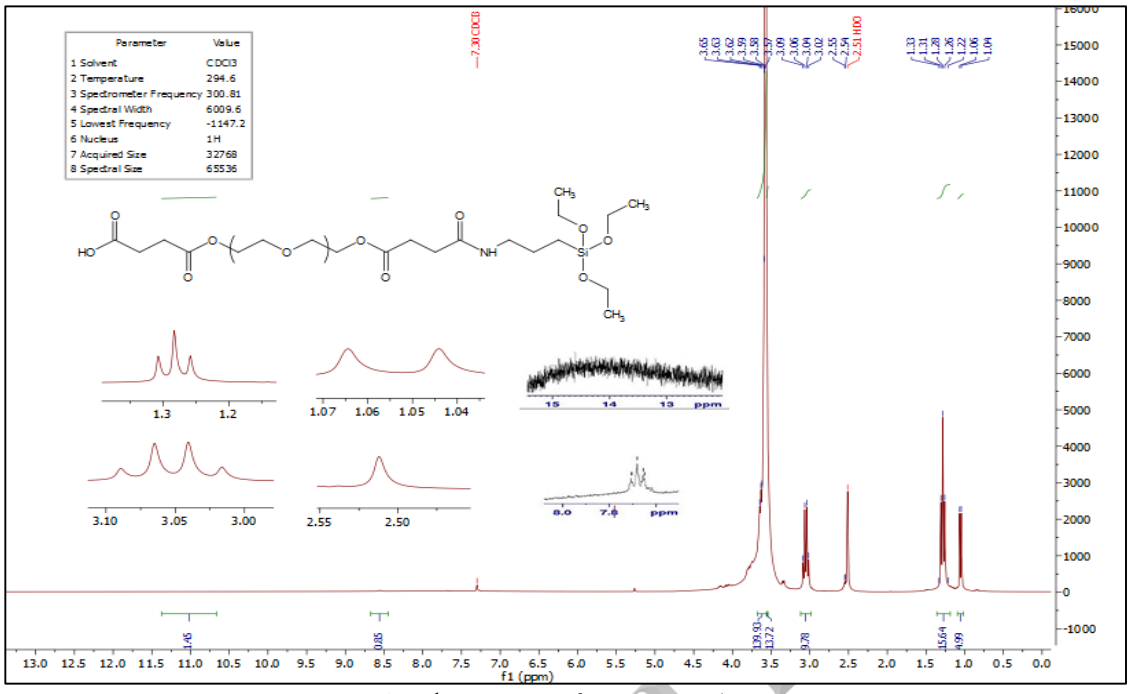

Fig. 7. ^{1}H NMR spectra for HOOC-PEG-silane

FT-IR analysis

The characteristic absorption peaks of Fe_3O_4f (a), HOOC-PEG-Silane (b), Fe_3O_4-PEG (c), and Fe_3O_4f-PEG-MET were identified through Fourier transform infrared (FT-IR) spectroscopy analysis (Figure 8). In the FT-IR spectrum of Fe_3O_4f fluidic (Figure 8a), the presence of Fe_3O_4 is confirmed by the band around 580–428 cm^{-1}, corresponding to the stretching vibration of Fe–O bonds. The peak at 3428 cm^{-1} is attributed to O–H stretching vibrations from hydroxyl groups present on the nanoparticles. Additionally, the stretching modes of citrate (COO^-) are observed at 1593 cm^{-1} and 1387 cm^{-1} [34, 39].

The peaks observed at 3405 cm^{-1} and 1730 cm^{-1} are attributed to the O–H and C=O functional groups of carboxylic acids, respectively. The peak at 1627 cm^{-1} corresponds to the C=O stretching vibration of the amide functional group. The peaks at 2937 cm^{-1} and 3374 cm^{-1} are attributed to C–H vibrations and N–H stretching from the amide bond of HOOC-PEG-APTES (Figure 8b). Additionally, the coordination between the two components is evidenced by the decrease in intensity and frequency of the hydroxyl and carbonyl groups (Figure 8c). The N–H and C–N stretching bonds from metformin are observed at 3136 cm^{-1} and 1405 cm^{-1}, respectively, while the bands at 3399 cm^{-1} and 3316 cm^{-1} are attributed to NH_2 stretching from metformin. Moreover, in Figure 8c, the Fe–O peaks shift from 428–580 cm^{-1} to 600–442 cm^{-1} due to coordination with compound b.

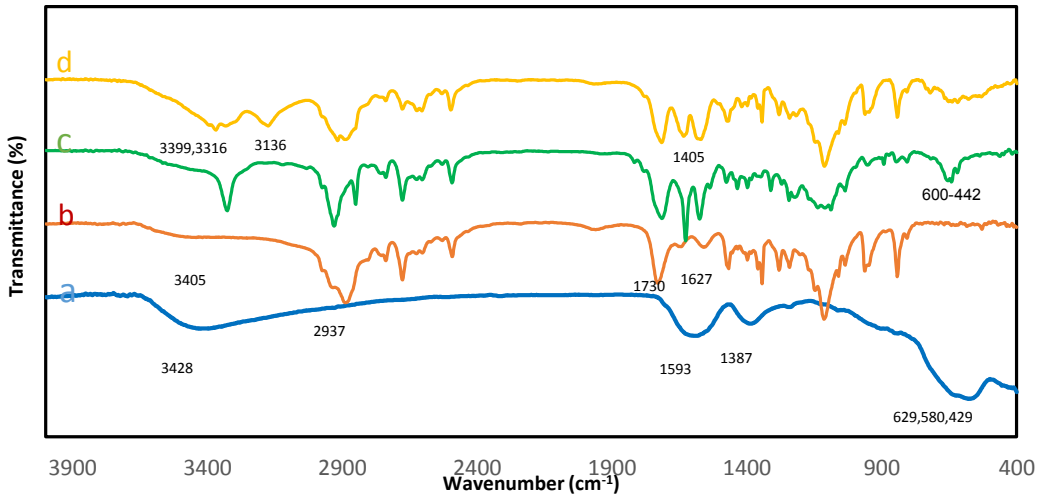

Fig. 8. FT-IR spectra of the Fe_3O_4f (a), HOOC-PEG silane (b), Fe_3O_4f-PEG (c) and Fe_3O_4f-PEG-MET (d). (**PEG**: Polyethylene glycol, **MET**: Metformin)

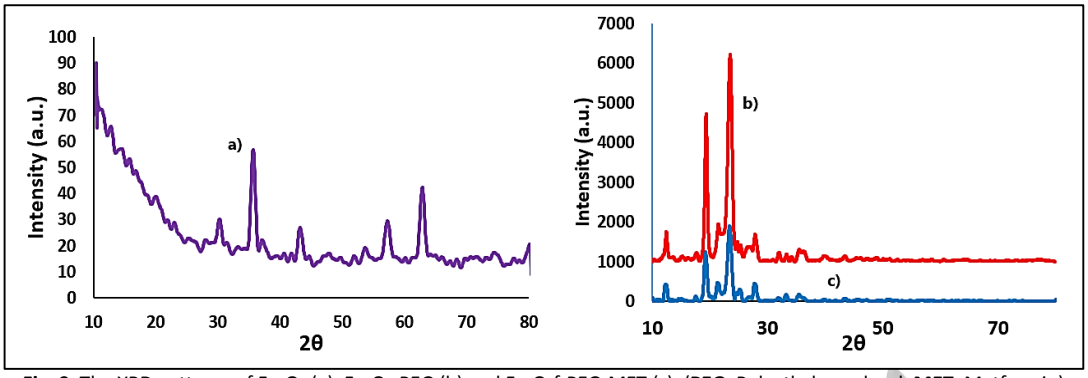

Fig. 9. The XRD patterns of Fe_3O_4 (a), Fe_3O_4-PEG (b) and Fe_3O_4f-PEG-MET (c). (**PEG**: Polyethylene glycol, **MET**: Metformin)

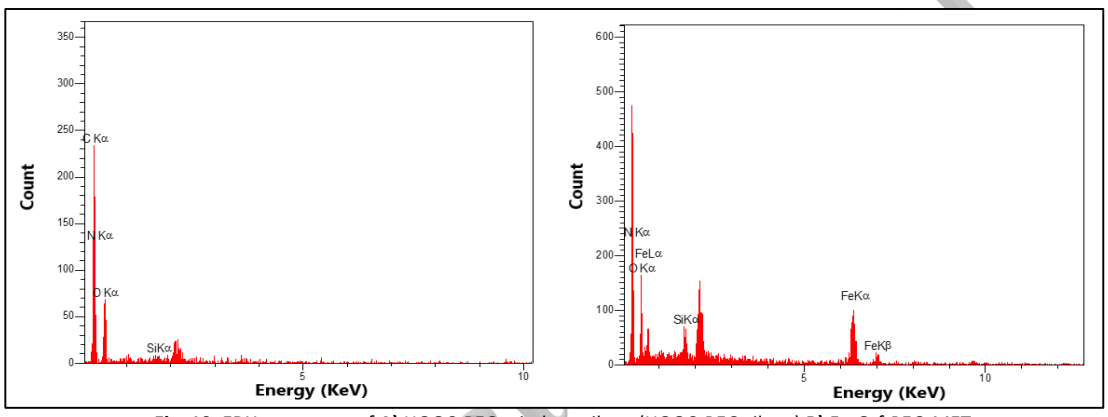

Fig. 10. EDX spectrums of **A)** HOOC-PEG-triethoxysilane (HOOC-PEG silane) **B)** Fe_3O_4f-PEG-MET

XRD analysis

The XRD patterns of Fe_3O_4f, Fe_3O_4-PEG, and Fe_3O_4f-PEG-MET are presented in Figure 9. As shown in Figure 9a, the characteristic peaks at 2θ = 30.18° (2 0 2), 35.42° (3 1 1), 43.18° (4 0 0), 53.54° (4 2 2), and 62.74° (4 4 0) are associated with the magnetorheological properties of Fe_3O_4 (Ref. Code: JCPDS:19-0629) [33]. In Figure 9b, in addition to the Fe_3O_4 diffraction peaks, peaks at 2θ = 19° and 23.4° correspond to PEG [45]. Finally, in Figure 9c, the diffraction peaks at 2θ = 16°, 21°, 23°, and 36° are attributed to the addition of metformin to the previous pattern [46].

As stated in Figure 9c, the intensity and position of the diffraction peaks changed due to the conjugation process of metformin.

In comparison, the crystallinity value and intensity of all peaks were reduced due to deformation of the bonding of metformin onto the PEG. The crystalline size of Fe_3O_4f NPs was estimated to be 87 nm in proportion to the Debye-Scherrer equation $d = K\lambda/(\beta\cos\theta)$.

EDX analysis

The types of elements in HOOC-PEG-triethoxysilane and Fe_3O_4f-PEG-MET structures were identified using the energy-dispersive X-ray (EDX) technique. This analysis was performed to confirm the synthesis and the presence of the magnetic core. In Figure 10a, the presence of nitrogen (N) and silicon (Si) indicates the composition of HOOC-PEG-triethoxysilane. In Figure 10b, the iron (Fe) peak, along with other elements, confirms the composition of the final blend.

VSM analysis

The magnetic properties of Fe_3O_4f NPs and Fe_3O_4f-PEG-MET were investigated using a vibrating sample magnetometer (VSM). As shown in Figure 11a, the samples exhibit superparamagnetic behavior. The saturation magnetization values for Fe_3O_4f NPs and Fe_3O_4f-PEG-MET were 50 emu/g and 0.06 emu/g, respectively (Figure 11).

The decrease in magnetic power is attributed to iron reduction. Additionally, ICP-OES analysis revealed that the amounts of iron and silicon in the final product were 0.07% and 0.42%, respectively.

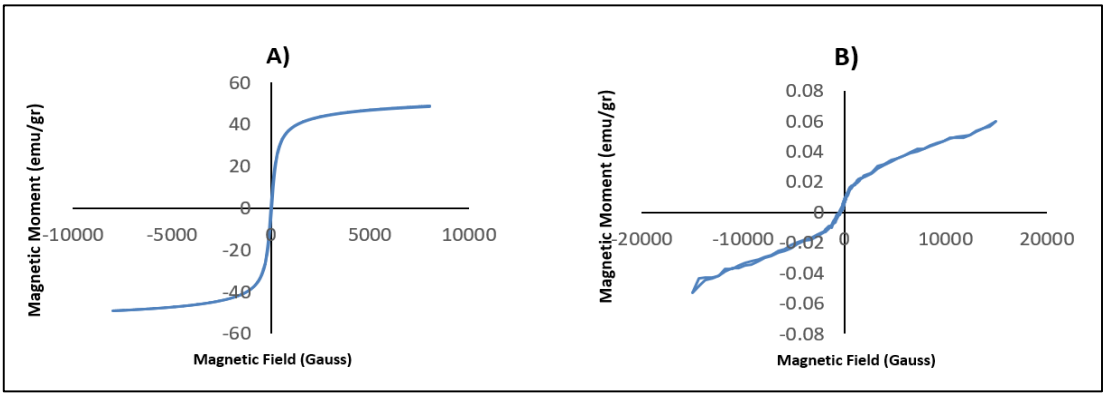

Fig. 11. The magnetization curve of **A)** ferrofluid or Fe_3O_4, **B)** Fe_3O_4f-PEG-MET (**PEG**: Polyethylene glycol, **MET**: Metformin)

In vitro evaluation of MPDT

In the literature, high-glucose culture medium is commonly used to model conditions similar to diabetes or more aggressive breast cancer in vitro. Unlike other breast cancer cell lines, such as MCF-7, high-glucose conditions lead to increased proliferation of MDA-MB-231 cells. This is primarily due to high glucose levels enhancing the expression of p38 phosphorylation, cyclin D1, and increased ERK phosphorylation in MDA-MB-231 cells [47].

Magnetic nanostructures, often in gold core-shell structures conjugated with sensitizing drugs, are typically used in optical treatments such as photodynamic therapy (PDT) or photothermal therapy. On the other hand, superparamagnetic nanostructures are more commonly employed in hyperthermia-based treatments due to their unique magnetic properties. In this study, a multifunctional magnetic nano-ferrofluid was used in photodynamic therapy for the first time.

The results in Figure 12 show that increasing the irradiation time in the MET, Fe_3O_4f-PEG, and Fe_3O_4f-PEG-MET treatment groups did not lead to a significant difference in survival rates. One reason for the absence of phototoxic effects in these groups is the lack of an absorption peak in the wavelength range of incoherent light radiation, meaning these compounds do not act as photosensitizers.

In contrast, increasing the irradiation time in the Fe_3O_4f-PEG-MET@MB group decreased survival, which can be attributed to the synergistic potential of methylene blue (MB) as a photosensitizer and metformin (MET) as a drug agent.

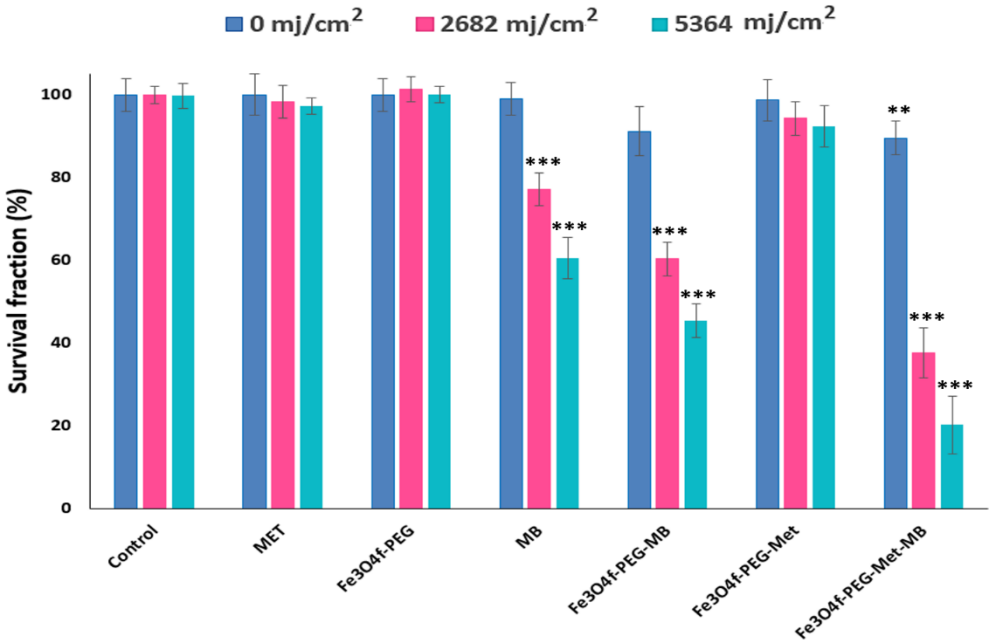

Fig. 12. The Survival fraction evaluation 24h after different irradiation conditions in in the presence of the agents at MD-MB-231 cells. Data has shown mean ± SD (n=*4*). (MB Concentration: 20µM, metformin: 1mM, Light source: 670 nm; 2682 mj/cm^2=3 min irradiation, 5364 mj/cm^2=6 min irradiation). (P<0.05: * , P<0.01: **, P<0.001:***)

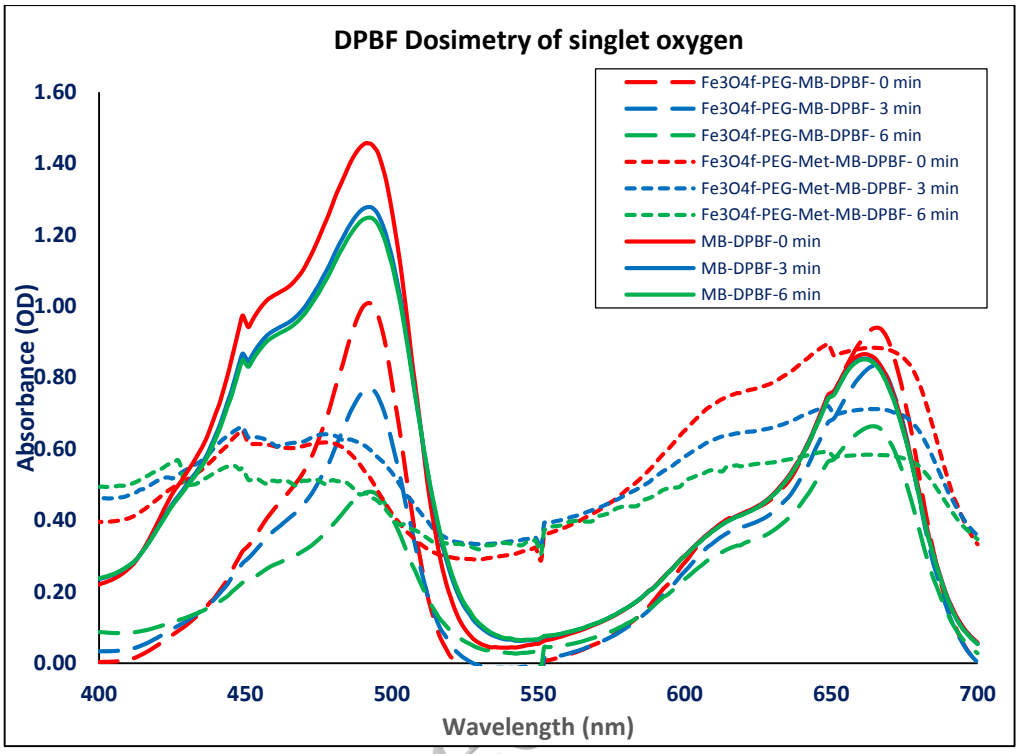

Fig. 13: DPBF dosimetry of ROS in different groups (Spectrophotometry analysis). (**MB**: Methylene Blue, **PEG**: Polyethylene glycol, **MET**: Metformin). As it can be seen, Fe_3O_4f-PEG-MB structure is more efficient in DPBF photobleaching than free MB. This phenomenon can be caused by two reasons: 1) Prevention of methylene blue photobleaching during irradiation. 2) Preventing the dimerization of methylene blue by conjugating it inside the nanostructure. The DPBF curve in the presence of Fe3O4f-PEG-MB-MET caused changes in its spectrum shape, which could be due to the strong interaction between these two structures.

Evaluation of ROS production during Photodynamic therapy

The results from the DPBF assay in Figure 13 show that in the groups containing MB, as the irradiation time increases, the rate of light bleaching of DPBF also increases. This is due to the higher efficiency of singlet oxygen production compared to free MB. MB is a dye that tends to undergo dimerization, which can affect its singlet oxygen production efficiency. However, by conjugating MB to the nanostructure, the decrease in efficiency caused by dimerization is nearly eliminated.

In the metformin group, the spectrum shape changes significantly with increasing irradiation time. This can be attributed to forming a new bond between metformin and the nanostructure or to chemical interactions affecting DPBF. The absorption spectrum of the DPBF-based structure serves as a typical representation for comparing singlet oxygen yield across different treatment groups containing photosensitizers. For better evaluation, the absorption peak of DPBF should be considered. A decrease or shift in the absorbance peak of DPBF (at 439 nm) indicates that the molecule is reacting with singlet oxygen. An increase in singlet oxygen production reduces the DPBF absorption peak, which is caused by the degradation of DPBF through its reaction with singlet oxygen and the photobleaching phenomenon [44].

DISCUSSION

Diabetic patients with aggressive breast cancer represent a major challenge for future treatment, as the complications of diabetes can exacerbate cancer progression, making it more aggressive and increasing the likelihood of metastasis. Therefore, the development of a nanopharmaceutical system designed to perform chemo-photodynamic multidrug therapy is a promising approach for treating tumors in patients with aggressive breast cancer, particularly those with underlying diabetes.

In this study, a new nanostructure was developed based on magnetic properties to address the challenges of non-reproducibility and weak biological stability of magnetic nanoparticles for drug delivery applications. These nanostructures are based on magnetic ferroelectrics, which are garnering significant attention due to their exceptional surface modification capabilities and long-term dispersibility. The magnetic ferrofluid, coated with PEG, maintains its magnetic properties and presents a promising candidate for multidrug

carrier systems in future theranostic applications. In this study, the Fe_3O_4f-PEG-MET-MB nanostructure was synthesized. After initial characterization and cytotoxicity assessment, the optimal concentration was selected and optimized for use in photodynamic therapy.

The size analysis results from the TEM method (Figure 4) indicated that the initial size of the magnetic nanoferrocell is approximately 100 nm. After surface modification and loading with metformin and MB, the final size increased to about 600 nm. Additionally, the FE-SEM results in Figure 6 revealed the spherical morphology and branched structure of the final nanostructure, with drug molecules positioned on the surface or between its branches. Numerous studies have shown that the size and shape of nanostructures are key factors in determining cellular uptake efficiency and their potential toxicity to living cells [48, 49]. Various studies have shown that small nanoparticles, ranging from a few nanometers to several hundred nanometers, enter cells through pinocytosis or macropinocytosis. It has also been reported that nanoparticles in the size range of 250 nm to 3 micrometers are primarily internalized through phagocytosis, while nanoparticles ranging from 120 to 150 nm are mainly internalized via clathrin- or caveolin-mediated endocytosis [50, 51]. Based on this model, it is predicted that the cellular uptake of Fe_3O_4f-PEG-MET-MB occurs primarily through phagocytosis or macropinocytosis. For clinical applications, nanostructures larger than 200 nm should generally be avoided for systemic injection, as they are more likely to be phagocytized by the immune system's macrophages or accumulate in the kidneys during excretion. Therefore, the size of this nanoconjugate should be further reduced in future clinical trials to enhance its suitability for therapeutic applications [52].

The presence of characteristic peaks for surface-modifying agents and drugs in the FT-IR, EDX, XRD, UV-Visible spectroscopy, and ^{1}H NMR spectroscopy confirms that the desired structure (Fe_3O_4f-PEG-MET-MB) has been successfully synthesized. Additionally, the VSM results in Figure 11, which were used to investigate the magnetic properties of the nanostructures, show that both ferrofluid nanoparticles and Fe_3O_4f-PEG-MET exhibit superparamagnetic properties. However, due to the substantial thickness of PEG, the saturation magnetization value of the fluid nanoparticles decreases from 50 emu/g (for Fe_3O_4) to 0.06 emu/g (for Fe_3O_4f-PEG-MET).

The results of photodynamic therapy in Figure 12 show that, initially, the selected concentrations of medicinal agents (MB concentration: 20 µM, metformin: 1 mM) do not exhibit cytotoxicity under dark conditions (without radiation). However, as the amount of radiation increases, cytotoxicity is observed to increase in the groups containing MB (MB groups, Fe_3O_4f-PEG-MB, and Fe_3O_4f-PEG-MET-MB).

To evaluate the performance of Fe_3O_4f-PEG-MET-MB as a nanocomplex for chemo-photodynamic therapy (PDT + local oxygen-generating drug such as metformin), different indices, including the TE and Syn, were defined. As previously mentioned, the TE index reflects the degree of effectiveness of Fe_3O_4f-PEG-MET-MB in enhancing photodynamic therapy performance compared to MB alone. A TE value greater than 1 indicates an enhancement of MB's photodynamic properties in the presence of Fe_3O_4f-PEG-MET. This enhancement could be attributed to metformin, which helps modulate the effects of hypoxia reduction during the photodynamic process.

Additionally, a synergism index greater than 1 (Syn > 1) indicates the presence of synergy in the treatment process. This index is complementary to the TE index, with the key difference being that it incorporates the contribution of other pharmaceutical factors to cell death in the fraction denominator.

As shown in Table 1, the TE and Syn indices are greater than one in all radiation conditions, with a slight decrease as radiation time increases. This phenomenon may be attributed to photosensitizer photobleaching or the activation of cancer cell resistance mechanisms.

Table 1: Different indices for evaluation of PDT efficiency in Fe_3O_4f-PEG-MET@MB groups

			Fe_3O_4f-PEG-MET@MB			
Exposure (mJ/cm²)	**CD ($MB_{20\mu M}$)**	**CD ($MET_{1\mu M}$)**	**CD (Fe_3O_4f − PEG)**	**CD (Fe_3O_4f − PEG − MET − MB)**	**Syn**	**TE**
2682	22.77	1.60	1.31	62.31	**2.70**	**2.73**
5364	39.48	2.75	0	79.75	**1.89**	**2.02**

$$\text{TE } (Fe_3O_4\text{f-PEG-MET@MB}) = \frac{CD(Fe_3O_4\text{f–PEG–MET@MB})}{CD(MB)}$$

$$\text{Syn } (Fe_3O_4\text{f-PEG-MET@MB}) = \frac{CD(Fe_3O_4\text{f–PEG–MET@MB})}{CD(MB) + CD(\text{MET}) + CD(Fe_3O_4\text{f–PEG})}$$

- **CD=** Cell Death, **MET=** Metformin, **MB=** Methylene Blue, **Fe_3O_4f=** Ferrofluids NP; Fe_3O_4 fluids NP, **Syn=** synergism index, **TE=** Treatment efficiency index

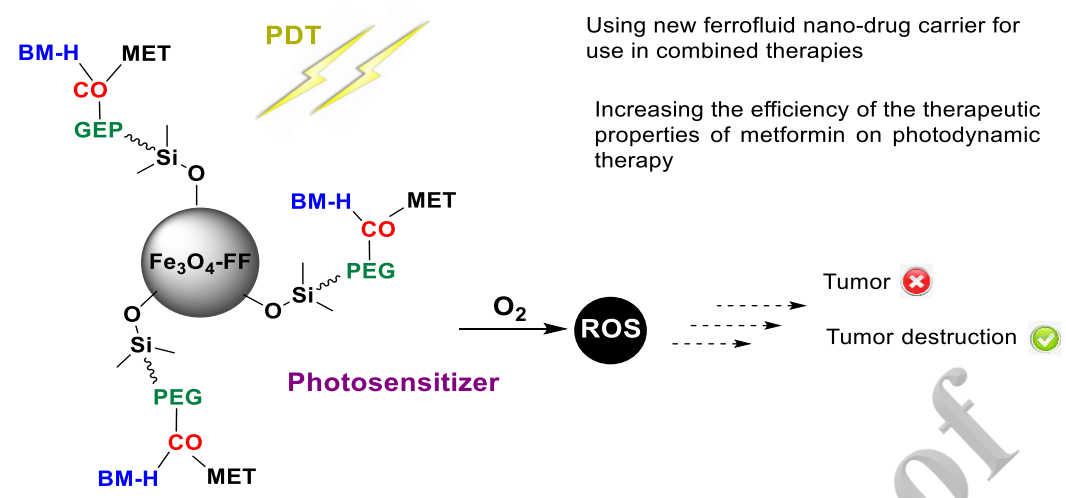

Fig. 14. Summarize the mechanism of CH-PDT

Few studies have explored the use of metformin in combination with photodynamic therapy. In the following section, key related studies are reviewed.

Osak et al. investigated the photodynamic effect of 5-aminolevulinic acid combined with metformin on KLN205 lung cancer cells using laser irradiation (630 nm, 1 and 5 J/cm²). They found that apoptosis and autophagy occurred in KLN205 cells following the combined treatment with 5-ALA-PDT and metformin. Their study also showed significant cytotoxicity when the metformin concentration was increased from 0.1 to 5 mM, in conjunction with 5 J/cm² of 5-ALA-PDT treatment [53].

Xiong et al. developed a composite by loading metformin and IR775 into a clinically applicable liposome, creating a two-in-one nanoplatform (IR775@Met@Lip) for photodynamic immunotherapy targeting bladder and colon cancers. They reported that IR775@Met@Lip could reverse tumor hypoxia, increasing ROS production and causing further chemical damage. Additionally, they found that photodynamic therapy (PDT) with IR775@Met@Lip (785 nm laser, 1 W/cm² for 150 s, Met concentration: 5 mM) also resulted in a reduction of PD-L1 overexpression [54].

Song et al. designed a multifunctional liposome in which hydrophilic metformin was encapsulated within the inner cavity, while hydrophobically modified chlorine e6 (Ce6) was incorporated into the outer membrane of the liposomes. Their study demonstrated that the nanoliposome carrying both metformin and Ce6 provides a novel strategy to enhance the effectiveness of photodynamic therapy (PDT) by modulating tumor oxygenation in breast cancer in mice (metformin = 16 mg/kg, Ce6 = 8 mg/kg, 660 nm laser for 30 min at a power density of 0.035 W/cm²).

The above studies confirm that the presence of metformin during photodynamic therapy can enhance photodynamic efficiency by modulating tumor hypoxia and reducing PD-L1 expression [55].

CONCLUSIONS

Effective management of cancer patients with coexisting diabetes requires individualized treatment protocols to optimize outcomes for both conditions. This is due to the complex interplay between cancer treatment and diabetes management, as cancer therapies can disrupt blood glucose homeostasis. In contrast, diabetes management can influence the efficacy of cancer treatments.

Cancer treatments, including radiation therapy, chemotherapy, and targeted therapies, can alter blood glucose levels by inducing insulin resistance and impairing insulin production. For example, radiation therapy can induce inflammation in the irradiated area, leading to insulin resistance and hyperglycemia in diabetic patients. Similarly, chemotherapy can cause insulin resistance and disrupt glucose metabolism, resulting in elevated blood glucose levels. As a result, healthcare professionals must closely monitor blood glucose levels in cancer patients with diabetes and adjust diabetes medications to manage the adverse effects of cancer treatment. Developing novel treatment strategies that address the unique challenges faced by cancer patients with diabetes is essential to optimize health outcomes, particularly for those with aggressive cancers, such as triple-negative breast cancer.

Type 2 diabetes is one of the most prevalent chronic diseases worldwide, affecting individuals across all age groups. Scientific evidence highlights a strong relationship between diabetes and the accelerated progression and increased invasiveness of various cancers. Among these, research has reinforced the link between diabetes and an increased risk of developing breast cancer, as well as its higher likelihood of metastasis. Studies indicate that breast cancer patients with diabetes have a 50% higher risk of dying from breast cancer compared to those without diabetes.

Some research implicates diabetes in the increased aggressiveness of triple-negative breast cancers (TNBC), which do not respond to conventional HER2/hormone-targeted therapies.

Given that MDA-MB-231 triple-negative breast cancer cells are highly resistant to metformin under hyperglycemic conditions, the Ch-PDT method offers a promising approach that can simultaneously utilize metformin (as an antidiabetic agent) and a photosensitizer in aggressive breast cancer patients. The factors predicting the enhanced effectiveness of the Fe_3O_4f-PEG-MET-MB nanostructure in photodynamic therapy include:

1) Improving cellular uptake of MB by micropinocytosis.

2) Occurrence of the effect of Ch-PDT as metformin causes disturbance in the mitochondrial respiration cycle and increases intracellular oxidative stress during photodynamic therapy.

PERSPECTIVE

The development of magnetic nano-ferrofluids opens up possibilities for combined theranostic applications, including photodynamic/photothermal therapy, magnetic hyperthermia, and magnetic resonance imaging. The goal of our research team in future studies is to develop a theranostic nanostructure based on magnetic ferrofluids for cancer treatment.

CONFLICT OF INTEREST

The authors declare that they have no conflict of interest or other disclosures.

FUNDING

This article is the result of a Ph.D thesis of a chemistry student of Ferdowsi University of Mashhad. The authors gratefully acknowledge the partial support of this study by Ferdowsi University of Mashhad Research Council (Grant no. p/3/54937). We also appreciate the medical physics research center of Mashhad University of Medical Sciences for their cooperation in carrying out the photobiological processes.

AUTHOR CONTRIBUTION

S.Ch, M.Gh, B.Akh: Designed the experiments; S.Ch, A.I: Performed experiments and collected data; S.Ch, M.Gh, B.Akh, A.I, A.S: Discussed the results and strategy; S.Ch, M.Gh, B.Akh, A.I, A.S: Writing an article; S.Ch, M.Gh: Directed and managed the study; S.Ch, M.Gh, B.Akh, A.I, A.S: Final approved of the version to be published.

REFERENCES

1. World Health Organization. The top 10 causes of death 2020 [Internet]. Available from: https://www.who.int/news-room/fact-sheets/detail/the-top-10-causes-of-death.
2. Bray F, Laversanne M, Sung H, Ferlay J, Siegel RL, Soerjomataram I, Jemal A. Global cancer statistics 2022: GLOBOCAN estimates of incidence and mortality worldwide for 36 cancers in 185 countries. CA Cancer J Clin. 2024;74(3):229-263.
3. Barone BB, Yeh HC, Snyder CF, Peairs KS, Stein KB, Derr RL, et al. Postoperative mortality in cancer patients with preexisting diabetes: systematic review and meta-analysis. Diabetes Care. 2010;33(4):931-939.
4. Leroith D, Scheinman EJ, Bitton-Worms K. The role of insulin and insulin-like growth factors in the increased risk of cancer in diabetes. Rambam Maimonides Med J. 2011;2(2):e0043.
5. Gallagher EJ, LeRoith D. The proliferating role of insulin and insulin-like growth factors in cancer. Trends Endocrinol Metab. 2010;21(10):610-618.
6. Hua H, Kong Q, Yin J, Zhang J, Jiang Y. Insulin-like growth factor receptor signaling in tumorigenesis and drug resistance: a challenge for cancer therapy. J Hematol Oncol. 2020;13(1):64.
7. Ma X, Nan F, Liang H, Shu P, Fan X, Song X, et al. Excessive intake of sugar: an accomplice of inflammation. Front Immunol. 2022;13:988481.
8. Sohrab SS, Raj R, Nagar A, Hawthorne S, Paiva-Santos AC, Kamal MA, et al. Chronic inflammation's transformation to cancer: a nanotherapeutic paradigm. Molecules. 2023;28(11).
9. Zhao H, Wu L, Yan G, Chen Y, Zhou M, Wu Y, Li Y. Inflammation and tumor progression: signaling pathways and targeted intervention. Signal Transduct Target Ther. 2021;6(1):263.
10. Volpe CMO, Villar-Delfino PH, Dos Anjos PMF, Nogueira-Machado JA. Cellular death, reactive oxygen species (ROS) and diabetic complications. Cell Death Dis. 2018;9(2):119.
11. Duan W, Shen X, Lei J, Xu Q, Yu Y, Li R, et al. Hyperglycemia, a neglected factor during cancer progression. Biomed Res Int. 2014;2014:461917.
12. Berbudi A, Rahmadika N, Tjahjadi AI, Ruslami R. Type 2 diabetes and its impact on the immune system. Curr Diabetes Rev. 2020;16(5):442-449.
13. Chang S-C, Yang W-CV. Hyperglycemia, tumorigenesis, and chronic inflammation. Crit Rev Oncol Hematol. 2016;108:146-153.

14. Shahid RK, Ahmed S, Le D, Yadav S. Diabetes and cancer: risk, challenges, management and outcomes. Cancers (Basel). 2021;13 (22).
15. Li W, Zhang X, Sang H, Zhou Y, Shang C, Wang Y, Zhu H. Effects of hyperglycemia on the progression of tumor diseases. J Exp Clin Cancer Res. 2019;38(1):327.
16. Feng JP, Chen JG, Yuan XL, Wang YP, Fang J, Liu C. Impact of 5-fluorouracil on glucose metabolism and pancreatic pathology in rats. Zhonghua Wei Chang Wai Ke Za Zhi. 2010;13(12):935-938.
17. Mahin D, Lavasani SM, Cristobal L, Tank Patel N, Sedrak M, Stewart D, et al. Hyperglycemia and glycemic variability associated with glucocorticoids in women without pre-existing diabetes undergoing neoadjuvant or adjuvant taxane chemotherapy for early-stage breast cancer. J Clin Med. 2023;12.(°).
18. Durrani IA, Bhatti A, John P. The prognostic outcome of 'type 2 diabetes mellitus and breast cancer' association pivots on hypoxia-hyperglycemia axis. Cancer Cell Int. 2021;21(1):351.
19. Natali A, Ferrannini E. Effects of metformin and thiazolidinediones on suppression of hepatic glucose production and stimulation of glucose uptake in type 2 diabetes: a systematic review. Diabetologia. 2006;49(3):434-441.
20. Pollak MN. Investigating metformin for cancer prevention and treatment: the end of the beginning. Cancer Discov. 2012;2(9):778-790.
21. Viollet B, Guigas B, Sanz Garcia N, Leclerc J, Foretz M, Andreelli F. Cellular and molecular mechanisms of metformin: an overview. Clin Sci (Lond). 2012;122(6):253-270.
22. Pollak M. The insulin and insulin-like growth factor receptor family in neoplasia: an update. Nat Rev Cancer. 2012;12(3):159-169.
23. Foretz M, Guigas B, Bertrand L, Pollak M, Viollet B. Metformin: from mechanisms of action to therapies. Cell Metab. 2014;20(6):953-966.
24. Kamarudin MNA, Sarker MMR, Zhou J-R, Parhar I. Metformin in colorectal cancer: molecular mechanism, preclinical and clinical aspects. J Exp Clin Cancer Res. 2019;38(1):491.
25. Rosilio C, Lounnas N, Nebout M, Imbert V, Hagenbeek T, Spits H, et al. The metabolic perturbators metformin, phenformin and AICAR interfere with the growth and survival of murine PTEN-deficient T cell lymphomas and human T-ALL/T-LL cancer cells. Cancer Lett. 2013;336(1):114-126.
26. Pei X, Wang X, Xian J, Mi J, Gao J, Li X, et al. Metformin and oxyphotodynamic therapy as a novel treatment approach for triple-negative breast cancer. Ann Transl Med. 2020;8(18):1138.
27. Dowling RJ, Zakikhani M, Fantus IG, Pollak M, Sonenberg N. Metformin inhibits mammalian target of rapamycin-dependent translation initiation in breast cancer cells. Cancer Res. 2007;67(22):10804-10812.
28. Foulkes WD, Smith IE, Reis-Filho JS. Triple-negative breast cancer. N Engl J Med. 2010;363(20):1938-1948.
29. Quinn BJ, Kitagawa H, Memmott RM, Gills JJ, Dennis PA. Repositioning metformin for cancer prevention and treatment. Trends Endocrinol Metab. 2013;24(9):469-480.
30. Nedylakova M, Medinger J, Mirabello G, Lattuada M. Iron oxide magnetic aggregates: aspects of synthesis, computational approaches and applications. Adv Colloid Interface Sci. 2024;323:103056.
31. Koksharov YA, Gubin SP, Taranov IV, Khomutov GB, Gulyaev YV. Magnetic nanoparticles in medicine: progress, problems, and advances. J Commun Technol Electron. 2022;67(2):101-116.
32. Esmaeilnezhad E, Choi HJ, Schaffie M, Gholizadeh M, Ranjbar M. Polymer coated magnetite-based magnetorheological fluid and its potential clean procedure applications to oil production. J Clean Prod. 2018;171:45-56.
33. Esmaeilnezhad E, Hajiabadi SH, Choi HJ. Effect of medium viscosity on rheological characteristics of magnetite-based magnetorheological fluids. J Ind Eng Chem. 2019;80:197-204.
34. Liang P-C, Chen Y-C, Chiang C-F, Mo L-R, Wei S-Y, Hsieh W-Y, Lin W-L. Doxorubicin-modified magnetic nanoparticles as a drug delivery system for magnetic resonance imaging-monitoring magnet-enhancing tumor chemotherapy. Int J Nanomedicine. 2016;11:2021.
35. Jeong YI, Kim DG, Jang MK, Nah JW. Preparation and spectroscopic characterization of methoxy poly(ethylene glycol)-grafted water-soluble chitosan. Carbohydr Res. 2008;343(2):282-289.
36. Liang PC, Chen YC, Chiang CF, Mo LR, Wei SY, Hsieh WY, Lin WL. Doxorubicin-modified magnetic nanoparticles as a drug delivery system for magnetic resonance imaging-monitoring magnet-enhancing tumor chemotherapy. Int J Nanomedicine. 2016;11:2021-2037.
37. Abdolahinia ED, Nadri S, Rahbarghazi R, Barar J, Aghanejad A, Omidi Y. Enhanced penetration and cytotoxicity of metformin and collagenase conjugated gold nanoparticles in breast cancer spheroids. Life Sci. 2019;231:116545.
38. Banerjee SS, Aher N, Patil R, Khandare J. Poly (ethylene glycol)-prodrug conjugates: concept, design, and applications. J Drug Deliv. 2012;2012.
39. Abdolahinia ED, Nadri S, Rahbarghazi R, Barar J, Aghanejad A, Omidi Y. Enhanced penetration and cytotoxicity of metformin and collagenase conjugated gold nanoparticles in breast cancer spheroids. Life Sci. 2019;231:116545.
40. Cecatto RB, de Magalhães LS, Rodrigues MFSD, Pavani C, Lino-dos-Santos-Franco A, Gomes MT, Silva DFT. Methylene blue mediated antimicrobial photodynamic therapy in clinical human studies: The state of the art. Photodiagn Photodyn Ther. 2020;31:101828.
41. Tardivo JP, Del Giglio A, De Oliveira CS, Gabrielli DS, Junqueira HC, Tada DB, et al. Methylene blue in photodynamic therapy: From basic mechanisms to clinical applications. Photodiagn Photodyn Ther. 2005;2(3):175-191.
42. Entradas T, Waldron S, Volk M. The detection sensitivity of commonly used singlet oxygen probes in

aqueous environments. J Photochem Photobiol B Biol. 2020;204:111787.
43. Chadwick SJ, Salah D, Livesey PM, Brust M, Volk M. Singlet oxygen generation by laser irradiation of gold nanoparticles. J Phys Chem C. 2016;120(19):10647-10657.
44. Mohseni H, Imanparast A, Salarabadi SS, Sazgarnia A. In vitro evaluation of the intensifying photodynamic effect due to the presence of plasmonic hollow gold nanoshells loaded with methylene blue on breast and melanoma cancer cells. Photodiagn Photodyn Ther. 2022;40:103065.
45. Barron MK, Young TJ, Johnston KP, Williams RO. Investigation of processing parameters of spray freezing into liquid to prepare polyethylene glycol polymeric particles for drug delivery. AAPS PharmSciTech. 2003;4(2):1-13.
46. Mokale V, Rajput R, Patil J, Yadava S, Naik J. Formulation of metformin hydrochloride nanoparticles by using spray drying technique and in vitro evaluation of sustained release with 32-level factorial design approach. Drying Technol. 2016;34(12):1455-1461.
47. Gupta C, Tikoo K. High glucose and insulin differentially modulates proliferation in MCF-7 and MDA-MB-231 cells. J Mol Endocrinol. 2013;51(1):119-129.
48. Chithrani BD, Chan WCW. Elucidating the mechanism of cellular uptake and removal of protein-coated gold nanoparticles of different sizes and shapes. Nano Lett. 2007;7(6):1542-1550.
49. Nel AE, Mädler L, Velegol D, Xia T, Hoek EMV, Somasundaran P, et al. Understanding biophysicochemical interactions at the nano-bio interface. Nat Mater. 2009;8(7):543-557.
50. Rejman J, Oberle V, Zuhorn IS, Hoekstra D. Size-dependent internalization of particles via the pathways of clathrin- and caveolae-mediated endocytosis. Biochem J. 2004;377(1):159-169.
51. Panariti A, Miserocchi G, Rivolta I. The effect of nanoparticle uptake on cellular behavior: disrupting or enabling functions? Nanotechnol Sci Appl. 2012;5:87-100.
52. Desai N. Challenges in development of nanoparticle-based therapeutics. AAPS J. 2012;14(2):282-295.
53. Osaki T, Yokoe I, Takahashi K, Inoue K, Ishizuka M, Tanaka T, et al. Metformin enhances the cytotoxicity of 5-aminolevulinic acid-mediated photodynamic therapy in vitro. Oncol Lett. 2017;14(1):1049-1053.
54. Xiong W, Qi L, Jiang N, Zhao Q, Chen L, Jiang X, et al. Metformin liposome-mediated PD-L1 downregulation for amplifying the photodynamic immunotherapy efficacy. ACS Appl Mater Interfaces. 2021;13(7):8026-8041.
55. Song X, Feng L, Liang C, Gao M, Song G, Liu Z. Liposomes co-loaded with metformin and chlorin e6 modulate tumor hypoxia during enhanced photodynamic therapy. Nano Res. 2017;10(4):1200-1212.